Romanian Reports in Physics **71**, 401 (2019)

TWO INSTANCES OF IMAGE SUPER-RESOLUTION USING SENSOR RASTER SCANNING AND DECONVOLUTION

P. C. LOGOFĂTU, V. DAMIAN, T. VASILE, M. L. PASCU

National Institute for Laser, Plasma and Radiation Physics, Laser Dept., str. Atomistilor nr. 409, P.O. Box MG-36, Măgurele, jud. Ilfov, Romania, 077125
E-mails: *petre.logofatu@inflpr.ro*; *victor.damian@inflpr.ro*; *tiberius.vasile@inflpr.ro*; *mihai.pascu@inflpr.ro*

Received June 26, 2018

Abstract. Super-resolution reconstructs a high-resolution image from one or more low-resolution recorded images. It uses a variety of hardware techniques, such as sensor raster scanning, or software techniques, such as interpolation, iterative back-projection, and the regularized methods, and it is useful in a variety of applications, such as video surveillance, medical diagnosis and remote sensing. Two applications based on the same technique are presented here in some detail: first, the hyperspectral characterization of a THz beam generated by a Time Domain Spectroscopy device and second, the resolution-enhanced photography. In both cases, images recorded by the sensor during a subpixel raster scan were interwoven in a high-resolution image, subsequently deconvoluted with a constant square kernel of the size of the sensor pixel. For hyperspectral characterization, regularization was necessary, whereas for resolution-enhanced photography, simple deconvolution sufficed. Magee's approach to super-resolution, which does not use convolution, was analyzed and rejected.

Key words: super-resolution, deconvolution, hyperspectroscopy.

1. INTRODUCTION

Despite the continuous increase in resolution of the recording devices, super-resolution is still very important in imaging for a lot of reasons. For instance, to guarantee the long-term stable operation of the recording devices, as well as the appropriate frame rate for dynamic scenes, digital surveillance products tend to sacrifice resolution to some degree [1]. This loss must be compensated somehow. In biology, quantitation of cellular data from light microscopy poses significant challenges. Interpolation increases spatial resolution and helps to define cell borders more accurately [2]. Therefore, super-resolution is still useful in a variety of applications such as video surveillance, medical diagnosis and remote sensing.

But there are more areas of interest. In this article two related instances of application of super-resolution are presented: 1) the hyperspectral characterization of the beam of the Time Domain Spectroscopy in the THz domain (TDS-THz), which is necessary in itself and is made difficult by the fact that at THz we are

close to the diffraction limit and the signal is low (with corresponding low signal to noise ratio – SNR) [3], and 2) the enhanced-resolution photography, necessary for the determination of the effect of point-spread function in a photography with the purpose of deblurring and depth determination within the photography [4].

Super-resolution imaging (also called subpixel estimation) reconstructs a high-resolution image from one or more low-resolution recorded images [1]. A lot of quite different techniques, hard and soft, enter under its umbrella. Among the hard methods, one can count the use of sophisticated sensors, such as the quincunx sensor [5, 6], or the interweaving of images obtained by subpixel raster scan [7]. Among the soft methods one can count interpolation, iterative back-projection, and the regularized methods. These techniques can often be combined [3, 7], as shown below.

In this paper a particular type of super-resolution technique consisting in a combination of hard and soft methods was used for two applications. The technique consists in subpixel sensor raster scanning and recording of low-resolution images in each of the raster positions (the hardware part), interweaving of the resulting images followed by deconvolution, necessary because the pixels are larger than the raster shifts (the software part). Sometimes one has to use regularized deconvolution in order to obtain satisfactory results.

In a partial manner and in a preliminary form, some of the results shown in subsubsections 2.1.1 and 2.2.1, and subsection 3.1 were previously shown elsewhere [3].

2. METHOD

2.1. THEORY

2.1.1. Sensor raster scanning and determination of subpixels

If one needs more resolution than the existing equipment affords, one can use the following technique (among others) that provides subpixel resolution. The sensor is shifted with fractions of the pixel size in a raster fashion and records images of low-resolution at each stop. For instance, in Fig. 1 the pixel is 4 times the size of the subpixel, hence the shifts are 1/4 pixel, horizontally and vertically. In Fig. 1a, for the illustration of the physical convolution, we need to show in the background an image of high resolution; we chose the image obtained at the end of the procedure, at sub-pixel resolution, because it makes the illustration of convolution more intuitive. Each pixel in Fig. 1b results by the integration of 4×4 subpixels from Fig. 1a. The window from Fig. 1a is moved in a raster fashion, horizontally and vertically with 1/4 of the window size. The low-resolution images are interwoven (or stitched) and the result is shown Fig. 1b, which is Fig. 1a convolved

with a kernel consisting in a constant matrix with all elements equal to 1/16. If we convert the low-resolution images into the matrices A^{kl}, then the equivalent matrix corresponding to the interwoven image, A^{iw} is written

$$A^{iw}_{(i-1)r+k,(j-1)r+l} = A^{kl}_{ij}, \quad i=1,\ldots,m, \quad j=1,\ldots,n, \quad k,l=1,\ldots,r\,. \tag{1}$$

where m and n are the dimensions of the low-resolution pictures, $r = 4$, and k, l are the raster indexes and correspond to the horizontal and vertical positions in the raster. Subsequently, the interwoven image is deconvolved and we obtain the desired high-resolution image from Fig. 1c. This method was used in reference [7]. Sensor raster scan was also used in references [5, 6], except they did not had to deal with convolution and deconvolution; the authors speculated the fact that the active area of the pixels of their sensor was less than half the total area of the pixel, and thus they could shift the sensor so that to cover an area of the image that the sensor did not record in the initial position.

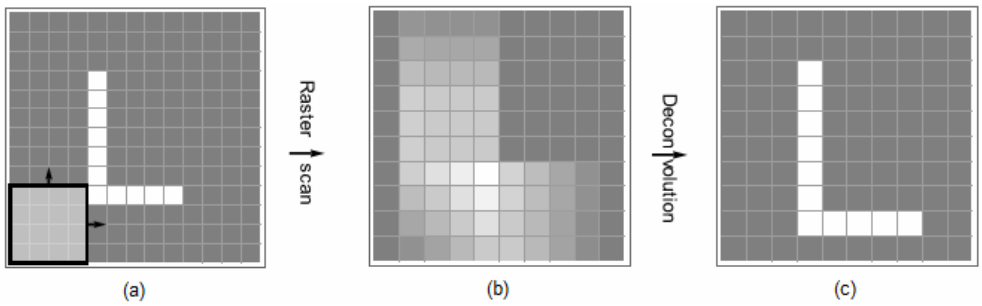

Fig. 1 – Illustration of the method: subpixel raster scan applied to an image with the desired subpixel resolution (a), image obtained by interweaving the low-resolution images (b), and deconvolved image (c). The pixel of the sensor is made out of 4 × 4 subpixels and determines the kernel of the convolution and deconvolution. Letter "L" was chosen for illustration purposes.

2.1.2. Magee's approach

Traditionally, the determination of the high-resolution image from the interwoven image has been written as equations with the pixel values of the high-resolution image as unknowns, and the values of the recorded low-resolution images as coefficients. With some boundary conditions these equations can be solved, giving pixel values of the high-resolution image. This approach has been undertaken by Magee [8], who used as boundary conditions the assumption that at least one row and one column have zero values in the low-resolution images. Magee's method is a sort of "poor man's deconvolution," having the advantage of intuitiveness.

Magee's method can be carried out in two ways. The first one, the way used by Magee himself, was to calculate the subpixels using the following recurrence relation between the elements of the high-resolution image matrix a

$$a_{ri+k-1,rj+l-1} = A_{ij}^{kl} - \sum_{p=1}^{r}\sum_{q=1}^{r'} a_{r(i-1)+k+p-1,r(j-1)+l+q-1}, \quad i=1,\ldots,m,\ \ j=1,\ldots,n,\ \ k,l=1,\ldots,r \tag{2}$$

with

$$r' = \begin{cases} r-1, & \text{for } p=r \\ r, & \text{in rest} \end{cases}. \tag{3}$$

The value of r' is such that in the sum in the right hand side of (2) the element of matrix a from the left hand side of (2) should not be present. It is assumed that the first $r-1$ rows and columns of a are 0, hence the recurrence relation (2) starts with a_{rr}. Obviously, if the matrices A^{kl} have say $m \times n$ elements, the matrix a has $rm \times rn$ elements.

The second way of performing the calculation of matrix a is through linear algebra calculations. First, we have to flatten matrix a and the interwoven matrices A^{kl}. Namely we set

$$a^{flat}_{(i-1)rn+j} = a_{ij}, \quad i=1,\ldots,rm,\ \ j=1,\ldots,rn, \tag{4}$$

$$A^{flat}_{[(i-1)r+k-1]nr+(j-1)r+l} = A_{ij}^{kl} = A^{iw}_{(i-1)r+k,(j-1)r+l}, \quad i=1,\ldots,m,\ \ j=1,\ldots,n,\ \ k,l=1,\ldots,r \tag{5}$$

Then we can finally write

$$A^{flat} = Ba^{flat}, \tag{6}$$

where B is a $r^2mn \times r^2mn$ matrix and a^{flat} and A^{flat} are r^2mn vectors. The matrix B is usually huge, typically it has easily in the order of 10^{12} elements. However, B can be constructed quite fast and easily in a recurrent manner, by taking advantage of its quasi-fractal pattern, the fact that all its non-vanishing elements are 1, and they are far less numerous than the zeros, *i.e.* B has high sparsity. It turns out that for large m and n, the ratio of ones over zeros is approximately $4/(m\,n)$, *i.e.* the number of ones is in the order of millions only, manageable even for a regular personal computer. In Fig. 2 is shown the structure of matrix B for the simplest case $m = n = r = 2$. After B is constructed, one can solve Eq. (6) using linear algebra numerical computational procedures, which are very fast when the matrix B is very sparse. They are especially fast if B has a band-diagonal form, and it does, due to the interweaving of A^{kl} as in Eq. (1). Actually, the linear algebra calculations take

much less computation time than the recurrence approach of Eq. (2), especially if we take into account the fact that, once the matrix B is calculated, it can be reused for any other case of identical m, n and r.

However, this approach is numerically very unstable. Noise perturbs very much the results. The method works fine when the data is completely noiseless, which unfortunately seldom happens. Deconvolution, especially regularized, is a much better approach. Of course, the recurrence and the matrix method for the determination of the subpixels is also a sort of deconvolution, but it is not as well protected from noise as actual deconvolution methods.

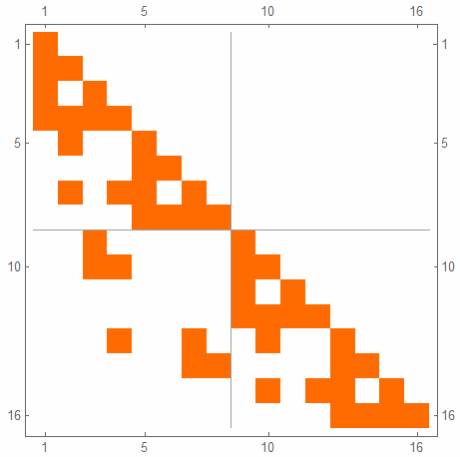

Fig. 2 – The matrix B for computing the subpixels when $m = n = r = 2$, the simplest case.

2.2. EXPERIMENTAL ARRANGEMENTS

2.2.1. TDS-THz

We characterized the beam of a THz-TDS system, the Ekspla THz kit with a FemtoFiber® laser produced by TOPTICA [9]. When the emission antenna is irradiated with a pulsed laser of 780 nm wavelength and 70 fs repetition rate, the system has an emission spectrum spanning 0.2-7.0 THz, enclosing the THz domain (0.3-3.0 THz). The detection in a TDS system is realized by synchronous detection of the signal with a lock-in amplifier. The phase-shift, for the synchronous detection, is introduced by the delay-line localized in the emitter arm. The TDS system samples the temporal shape of the electromagnetic pulse at equal time shifts. This data is then Fourier transformed and the frequency spectrum is obtained. The entire system is controlled by a computer.

The region of the beam to be measured is selected by means of an electromechanical scanning mechanism SM (part of the THz kit) equipped with an opaque screen having carved at its center a square aperture, which acts as a mobile collecting window of 12 × 12 mm for the detector; the aperture also acts as a mobile mask for the image.

2.2.2. Photography

The finest detail in an image is a pixel, which corresponds to a cell-like element called photo-site in the sensor, which for convenience is also called pixel sometimes. The value recorded by a photo-site, i.e. of the pixel is the integration of the light intensity over the active area of the photo-site, and it depends on its physical size and shape. To improve the level of detail in an image, it is required a decrease of the photo-site size, i.e. a different type of imaging sensor. However, it is possible to obtain the same information as if the photo-site was smaller by a computational method of super-resolution, by shifting the sensor in the image plane of a photo lens with fractions of pixel, which are equal to the desired subpixel size. For subpixel computation a sensor with a large active area, a fill factor as close to 100% as possible, is required. Also, it should be a black and white sensor, without color filters. The sensor we used in our experiments, a CCD camera DCU223M from Thorlabs [10] is such a sensor. The CCD was attached to a XY high-resolution motorized, electro-mechanical translation stage from Prior Scientific [11]. In front of it was placed a photographic objective, and in front of the objective, the test pattern. We aligned the system so that the test pattern is imaged on the sensor. Then the translation table was moved in a 4 × 4 raster manner with shifts of one quarter of a pixel (1/4 px), and pictures of 1024 × 768 pixels were taken at the 16 stops. They were interwoven together in one high-resolution image that looks much smoother but blurred. Then the interwoven image was deconvolved using a kernel consisting of a 4×4 identical matrix having all elements equal to 1/16.

In order to avoid the backlash error, the translations on vertical (Y) direction were made on the same sense every time. For the translations on the horizontal (X) direction, we could not avoid turning back, so we monitored (and measured) them using a SIOS interferometer. Prior to experiment, a stage calibration was achieved. The translation offset was measured with a traceable length measurement interferometer SIOS and for a step of 1.16 μm the offset measured ~0.1 μm.

In order to properly apply this method some considerations must be taken into account. First, the sensor electrical parameters (exposure, gain, etc) need to be exactly the same for the acquisition of all 16 frames. The acquisition is slow, it requires some time due to translation delays from one frame to the next and consequently the system must be static for the duration.

3. APPLICATIONS

3.1. HYPERSPECTRAL CHARACTERIZATION OF A THz BEAM

One stumbling block for THz imaging is the difficulty of working with the radiation source. THz sources are not user-friendly, certainly less easy to use than monochromatic radiation sources of visible light, ordinarily used for imaging. The wavelengths involved are very long (hundreds of micrometers, millimeters), and thus the diffraction limit makes them unsuitable for the observation of small details. The very shape of the THz pulse, *i.e.* its spatial distribution is not well controlled or even known. For these reasons, the characterization of the beam profile for THz radiation is important. Another problem is the low signal of the TDS, on the order of μW. One can increase both the signal value and the SNR by increasing the collecting window of the TDS sensor, but then the imaging resolution decreases.

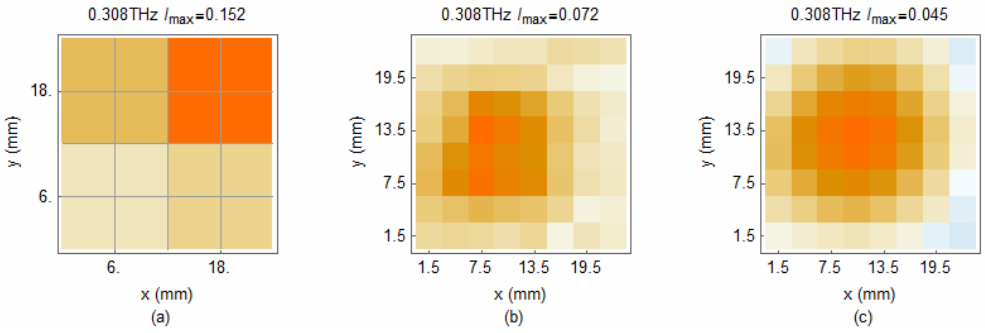

Fig. 3 – The stages of the procedure for obtaining high-resolution images of the THz beam. Comparison between (a) one of the 16 low-resolution images, (b) the resulting image after interweaving the low-resolution images and (c) the high-resolution image, interwoven and deconvoluted with regularization. The pale blue color of some pixels indicates slightly negative values.

In our work, we used deconvolution as a technique for subpixel estimation in THz imaging. We used deliberately a detector with a large square collecting window, whose parameters are known and controlled (12 × 12 mm). Increasing the size of the convolution kernel (the window), as we did, makes the convolution effect even worse, but now we know *a priori* the nature of this effect and how to correct it. Moreover, this way we avoid crossing the resolution limit. In Fig. 3 are indicated the steps of the procedure for obtaining a high-resolution image although in the normal operation mode the system records only low-resolution images or high-resolution blurred images. They are the steps described in subsubsection 2.1.1, but applied to the particular case of hyperspectral THz beam characterization. The target resolution is 3 × 3 mm.

In Figs. 3 and 4 we used a color code we think is quite intuitive. Warm colors represent positive values and cold colors negative values. The more intense and saturate a color is, the higher is the absolute value and *vice versa*.

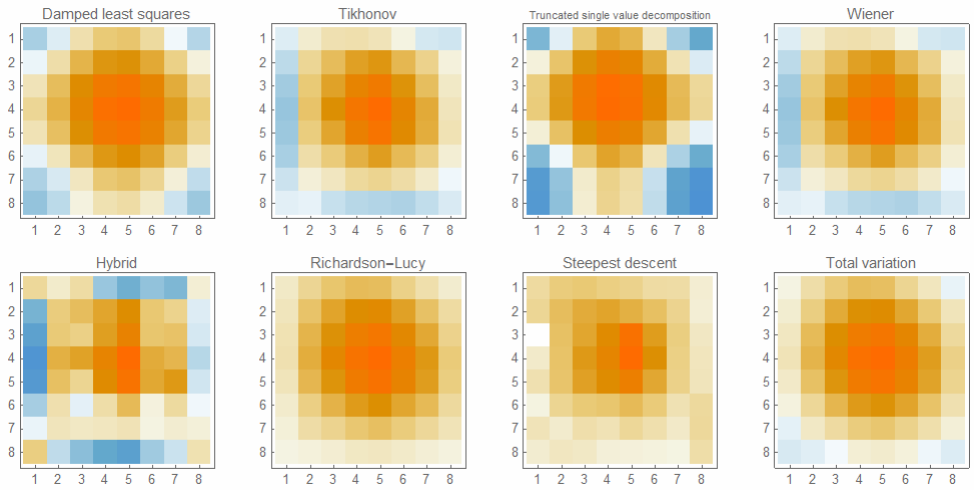

Fig. 4 – Comparison between the results obtained using various regularized deconvolution methods. One may notice that the best method seems to be the total variation, with Richardson-Lucy as second best. The frequency of 0.308 THz was chosen for illustration. Blue represents negative values.

The acquired THz image seemed to be strongly affected by noise and other perturbation factors. Therefore, we had to try various deconvolution methods with specific features for diminishing the influence of the noise in the reconstructed image. Figure 4 illustrates the results obtained *via* the following methods: the damped least-squares (the Levenberg-Marquardt algorithm) [12], the Tikhonov regularization [13], the truncated single value decomposition regularization [14], the Wiener filter [15], the Tikhonov-Golub-Kahan bidiagonalization regularization or the hybrid method [16], Richardson-Lucy [17], the modified residual norm steepest descent [18], and the total variation norm regularization [19]. In choosing the right method for signal deconvolution we were guided by three criteria: the method had to be designed specifically for the problems of which we were aware, it had to yield a final image that made sense (highly negative intensities were reason for summary rejection) and must have a robust convergence to the correct solution. It turned out that the best method was the total variation norm regularization with Richardson-Lucy as second best.

All the examples shown in Figs. 3 and 4 are for the frequency of 0.308 THz, but we applied the same procedure to all frequencies. The result was that for the lower frequencies the beam had Gaussian intensity distribution, as in Fig. 3c.

The waist of the beam increased with frequency and the center of the Gaussian wobbled slightly. For high frequencies, the results did not make sense and we discarded them.

3.2. RESOLUTION-ENHANCED PHOTOGRAPHY

A total of $4 \times 4 = 16$ low resolution images differing from each other by incremental shifts of pixel/4 in the horizontal and the vertical direction were recorded, then interwoven and deconvoluted. The pixilation effect in the zoom is visible in Fig. 5a, *i.e.* the picture fragment is of low resolution. Figure 5b was obtained by interweaving the 16 low resolution images, in the manner indicated in Eq. (1). Figure 5b shows high resolution, it is smooth, free of pixilation. However, it is blurred, namely convoluted with a rectangular constant kernel of 4×4 subpixels. Figure 5c is a fragment of the image obtained by deconvolving the interwoven image of which Fig. 6b is a fragment.

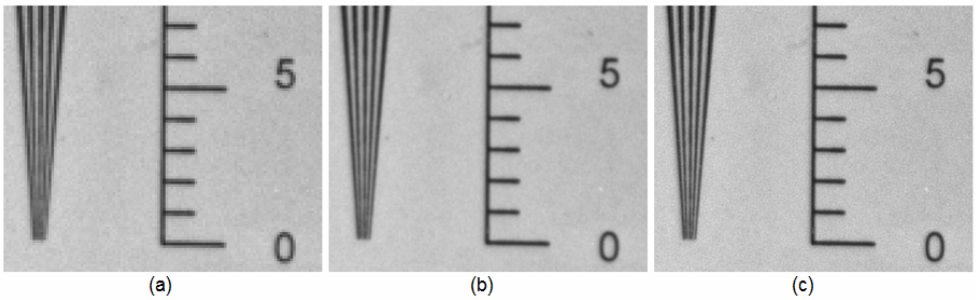

Fig. 5 – Enhanced-resolution photography. Comparison between zooms of (a) one of the 16 low-resolution images, (b) the low-resolution images interwoven into one image (the image is high-resolution but blurred), and (c) the high-resolution image, interwoven and deconvoluted.

We tried Magee's method for the data shown in Fig. 5 but the results (shown in Fig. 6) were poor. The problem with this method seems to be that, in the calculations, the absolute values of the noise add up, and the sum is alternatively added to and subtracted from the true values of the subpixels. This is illustrated by the fact that when we average the subpixels in cells of 2×2 subpixels, as in Fig. 6a, (or any other combination of even numbers of rows and columns of subpixels) the noises from adjacent subpixels cancel each other out and we obtain an image close to that of Fig. 5c. In Fig. 6b the calculated picture is shown without averaging and it is a sort of chess table with red pixels (high positive value) and green pixels (high negative value). Therefore, one can obtain meaningful pictures with this method, but at the price of sacrificing resolution, contradicting the very reason for which we started this research.

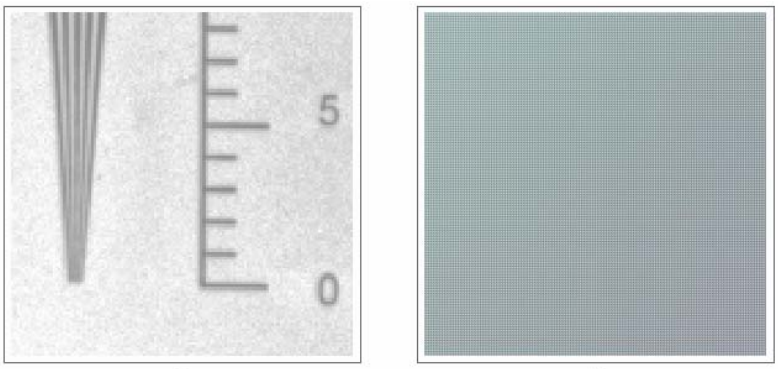

Fig. 6 – Noisy images obtained using Magee's method: with averaging of the subpixels (a), and without averaging (b).

Enhanced-resolution photography is useful for instance for the determination of the effect of point spread functions in a photography, which can be critical to deblurring and obtaining the depth of the details from the photography [4].

4. CONCLUSION

We analyzed theoretically and implemented experimentally a super-resolution imaging technique consisting in the shifting of the sensor with fractions of pixel (which are the subpixels) in a raster manner and recording low-resolution images in each position, interweaving the low-resolution images into one, and applying to it deconvolution with a constant kernel having the size of the (low-resolution) pixel. The technique was demonstrated for two particular cases: the hyperspectral characterization of a THz beam generated by a TDS and the enhancement of the resolution of photography. For hyperspectral characterization, regularization was necessary, but for resolution-enhanced photography, simple deconvolution was enough. The best deconvolution method turned out to be the total variation method with Richardson-Lucy the second best. Also, the THz beam was approximately Gaussian for low frequencies, but the analysis did not turn up usable results for high frequencies. The waist of the Gaussian increased slightly with frequency while the position of the center wobbled slightly. In photography sensor raster scan increased the resolution, illustrated by the fact that the pixilation effects visible in a zoom, were eliminated. Magee's method, in which the deconvolution is replaced by solving a system of equations, was also tried, but with poor results. Magee's method was proven to be very sensitive to noise, which tends to add up with alternative signs to adjacent subpixels in the final image. Averaging the subpixels in cells of even number of rows and columns eliminated the oscillations, but any gain in resolution was also lost.

Acknowledgments. This work was partially financed by the Unitatea Executiva pentru Finantarea Invatamantului Superior under grant 290/2014 INFLPR-ISS-UEFISCDI "THz-Detect" and partially by the Autoritatea Naţională pentru Cercetare Ştiinţifică in the frame of the Nucleus program - contract 4N/2016.

REFERENCES

1. S. Hofmann and G. Münzenberg, Rev. Mod. Phys. **72**, 733–756 (2000).
2. L. Yue, H. Shen, J. Li, Q. Yuan, H. Zhang AND L. Zhang, Signal Process **128**, 389–408 (2016).
3. J. M. Guberman, A. Fay, J. Dworkin, N. S. Wingreen, Z. Gitai, PLOS Comput Biol **4**, e1000233 (2008).
4. P. C. Logofătu and V. Damian, J. Opt. **20**, 055701 (2018).
5. A. Levin, R. Fergus, F. Durand and W. T. Freeman, SIGGRAPH '07 Conference, San Diego, CA, (USA) – August 05–09, 2007, art # 70.
6. C. Latry and B. Rougé, Proceedings of the International Geoscience and Remote Sensing Symposium (IGARSS), Toulouse, France, pp. 315–317 (2003).
7. T. Vasile, V. Damian, M. Vasile and D. Coltuc, Rom. Rep. Phys. **69**, 804 (2017).
8. M.-J. Sun, M. P. Edgar, D. B. Phillips, G. M. Gibson and M. J. Padgett, Opt. Express **24**, 10476–10485 (2016).
9. M. L. Magee, Fourth Internat. Joint Conf. Pattern Recognition Kyoto, 1978, pp. 521–524.
10. http://www.ekspla.com/wp-content/uploads/2011/05/thz-emitter-and-detector-for-800-nm-wavelength-lasers.pdf.
11. https://www.thorlabs.com/newgrouppage9.cfm?objectgroup_id=2916.
12. https://www.prior.com/product-category/motorized-stages.
13. W. H. Press, S. A. Teukolsky, W. T. Vetterling and B. P. Flannery, *Numerical recipes in C++: The art of scientific computing*, Cambridge, Cambridge University Press, pp. 811–7 (2002).
14. P. C. Hansen, SIAM Journal on Scientific and Statistical Computing **11**(*3*), 503–518 (1990).
15. G. Golub, W. Kahan, J. SIAM Numer. Anal. Ser. B **2**(*2*), 205–24 (1965).
16. L. R. Lines and S. Treitel, Geophysical Prospecting **32**, 159–86 (1984).
17. R. Yarlagadda, IEEE Transactions on Acoustics, Speech, and Signal Processing ASSP-**33**(*1*) 174–82 (1985).
18. W. H. Press, S. A. Teukolsky, W. T. Vetterling and B. P. Flannery, *Numerical recipes in C++: The art of scientific computing*, Cambridge University Press, Cambridge, 2002, pp. 552–555.
19. W. H. Richardson, J. Opt. Soc. Am. **62**, 55–59 (1972).
20. T. F. Chan and C.-K Wong, IEEE T. Image Process. **7**(*3*) 370–75 (1998).